HHS Public Access

Author manuscript

J Struct Biol. Author manuscript; available in PMC 2021 August 31.

Published in final edited form as:

J Struct Biol. 2020 November 01; 212(2): 107607. doi:10.1016/j.jsb.2020.107607.

Phosphatidylserine-enriched monolayers controls calcium phosphate nucleation and growth: a physicochemical understanding of matrix vesicles mineralization

Marcos A. E. Cruz[1], **Claudio R. Ferreira**[1], **Camila B. Tovani**[1], **Flávia A. de Oliveira**[2], **Maytê Bolean**[1], **Luciano Caseli**[3], **Saida Mebarek**[4], **José Luis Millán**[2], **Rene Buchet**[4], **Pietro Ciancaglini**[1,*], **Ana Paula Ramos**[1,*]

[1]Faculdade de Filosofia, Ciências e Letras de Ribeirão Preto, FFCLRP - Universidade de São Paulo – Departamento de Química, Brasil

[2]Sanford Burnham Prebys Medical Discovery Institute, La Jolla, CA 92037, USA

[3]Institute of Environmental, Chemical and Pharmaceutical Sciences - Federal University of Sao Paulo, Brazil

[4]Universite de Lyon, ICBMS UMR 5246 CNRS, Villeurbanne, France

Abstract

Bone biomineralization is an exquisite process by which cells control the synthesis and organization of a hierarchically mineralized matrix. Growing evidence has uncovered the involvement of one class of extracellular vesicles, the matrix vesicles (MVs), in the formation and delivery of the first mineral nuclei to the bone growth front. MVs are nanoreactors equipped with specific biochemical machinery and released by mineral-competent cells and to initiate mineral formation. However, little is known about the pathways by which MVs can template and trigger this process. Here, we present a combination of *in situ* investigations and *ex vivo* analysis of MVs extracted from growing-femurs of chicken embryos to investigate the role played by phosphatidylserine (PS) in the formation of the mineral nuclei. By using self-assembled Langmuir monolayers, we reconstructed the nucleation core- a PS-enriched motif present inside MVs and already thought to be the entity responsible to trigger mineral formation during mineralization. *In situ* infrared spectroscopy of Langmuir monolayers and *ex situ* analysis by transmission electron microscopy evidenced that mineralization was achieved within 240 min on supersaturated solutions only when PS was present. Amorphous calcium phosphate nucleated by PS was converted into biomimetic apatite after 24 h of incubation. By using monolayers containing lipids extracted from native MVs, mineral formation was also achieved after 240 min in a manner that resembles the artificial monolayers containing PS. We raise the possibility that PS-mediated nucleation could be a predominant pathway to produce the very first mineral in the bone/cartilage mineralization.

*corresponding authors: pietro@ffclrp.usp.br, anapr@ffclrp.usp.br.

Keywords

matrix vesicles; Langmuir monolayers; phosphatidylserine; biomineralization; calcium phosphate

1. Introduction

Biomineralization of hard tissues such as bone and dentin takes place during its formation, development, remodeling and repair, being remarkable for involving a complex spatio-temporal sequence of events regulated by bone-forming cells. However, a big question that still perdures on the understanding of bone formation, is the origin of the mineral phase. Seeking to overcome an inhibitory barrier that limits the amount of free calcium and phosphate ions, cells must work in orchestration to trigger the accumulation of these ions in a very regulated spatio-temporal manner(Reznikov et al., 2020).

Matrix vesicles (MVs) are mineralizing extracellular vesicles thought to be responsible to initiate the precipitation of the very first mineral nuclei on bone biomineralization. (Anderson, 1967) and (Bonucci, 1967) individually visualized mineral-related particles in mineralized cartilage using electron microscopy, which were later recognized as mineralizing MVs. Despite over 50 years of studies, questions about the detailed mechanism(s) by which MVs are secreted and initiate mineralization remain elusive (Wuthier and Lipscomb 2011; Bottini et al. 2017). The *in vivo* identification of MVs under native conditions, differentiate them from other extracellular vesicles and the precise characterization of mineral formation mediated by these structures *in vitro* are the main challenges that created skepticism from several researchers regarding the function of MVs on bone formation.

MVs act as a smart nanoreactor due to two main properties: they display an elegant enzymatic machinery working in orchestration to control the phosphate/pyrophosphate ratio; and mineral formation on MVs can be specifically templated by their lipid/protein composition. The biochemical machinery of MVs is quite complex. Regarding the control of phosphate/pyrophosphate ratio, two phosphatases, namely, orphan phosphatase 1 (PHOSPHO1) and alkaline phosphatase (ALP) act in concert with a third enzyme, ectonucleotide pyrophosphatase/phosphodiesterase 1 (ENPP1), each one producing or hydrolyzing phosphate (Pi) and pyrophosphate (PPi) necessary to achieve concentrations required to trigger mineralization (Dillon et al., 2019; Millán, 2013). MVs are also enriched in phosphate transporters (Beck, 2019), and annexins that might be involved in the binding and transport of Ca^{2+} to the inward of MVs (Bolean et al., 2015; Bottini et al., 2018). Lastly, MVs have specific lipid composition that differentiate them from their progenitor cells (Abdallah et al., 2014). The specific lipid content is an important modulator of their enzymatic activity/function (Bolean et al., 2020, 2010; Derradi et al., 2019; Favarin et al., 2020; Simão et al., 2010). This complex enzymatic machinery is required to trigger a local Pi/PPi ratio control, increasing the local supersaturation of Ca^{2+} and Pi and mediating the collagen mineralization.

There is growing evidence of the involvement of extracellular vesicles on the mediation of collagen mineralization, which highlights the importance of studying the pathways

by which MVs control mineral nucleation. MVs have been observed *in vivo* strongly attached to collagen fibrils (Anderson et al., 2004). Moreover, mineral bodies have been observed translocated from inside the cells to the extracellular matrix (Boonrungsiman et al., 2012; Iwayama et al., 2019; Kerschnitzki et al., 2016; Mahamid et al., 2011b, 2010). The composition of these structures, i.e., their protein and lipid content, was not determined in these studies, so it is not possible to relate them to MVs. On top of that, it has been proposed a mitochondrial origin for mineral-loaded vesicles (Boonrungsiman et al., 2012; Iwayama et al., 2019; Pei et al., 2018), but the relation of these structures with MVs or if MVs could be originated from a mitochondrial pathway is still debatable. Independently of nomenclature/biogenesis pathway, these studies revealed that extracellular vesicles could control biomineral precursor phase nucleation and further deliver to propagate collagen mineralization. In case of MVs, it has been proposed that the nucleation ability resides in a nucleation core inside their lumen, that nucleates calcium phosphate by a phospholipid-dependent manner(Jiao et al., 1997).

The idea that phospholipids could control the nucleation of calcium phosphate started from seminal studies of bone ultrastructure by histological and lipid solubilization of mineralizing epiphyseal cartilage (Irving and Wuthier, 1968; Wuthier, 1969). Observing that most part of phospholipids were closely associated with the newly mineral phase formed in the primary ossification and that, upon increased mineralization, these lipids could only be extracted after tissue demineralization (Wuthier, 1971), it was postulated that phospholipids, mainly acidic ones, might play a role in the ossification (Cotmore et al., 1971). Phospholipids associated to minerals were later extracted from mineralized tumor (Anghileri and Dermietzel, 1973) and calf bone (Boskey and Posner, 1975) revealing that these complexes could be an integral entity of bone. It was discovered them the existence of a PS-enriched acid-labile structure in the lumen of MVs(McLean et al., 1987; Register et al., 1986) responsible for their nucleation ability. This PS-enriched structure inside the MVs is called nucleation core. Characterization of isolated nucleation core from native MVs revealed to be composed by ~1 nm diameter subunits formed by clusters of Ca^{2+} and phosphate ions, and amorphous calcium phosphate (ACP) its major mineral component (Wu et al., 1997).

The nucleation core of MVs have been extensively studied *in vitro* by Wuthier's group (Genge et al., 2007; Wu et al., 2009, 2008, 1996). These studies advanced to demonstrate that PS is the major entity responsible for the mineralization ability of the nucleation core. Their approach was to recreate the nucleation activity of MVs by adding PS in supersaturated solutions. From this, several features, such as the reduction of the nucleation efficiency of PS in presence of other phospholipids or some cations (e.g. Mg^{2+} and Zn^{2+}) were determined. Moreover, the nucleation ability of PS can be triggered by addition of highly charged proteins (i.e. annexin). All these characteristics, as known nowadays, are indicative of an amorphous-mediated pathway. However, earlier studies on reconstitution of the nucleation core were performed only in bulk solution, which do not determine the importance of the interfacial processes, and lack in the analysis of the process by a multistep crystallization point-of-view.

To further delineate mechanisms of calcium phosphate nucleation and growth in PS-enriched interfaces, we explored calcium phosphate nucleation using Langmuir monolayers. The advantages of this technique are the possibility of accessing thermodynamic parameters associated to the accurate control of the composition and the organization of the monolayer while allowing the coupling of several techniques for *in-situ* characterization (Caseli et al., 2015; Derradi et al., 2019). Thus, we mimetized the mineral triggering ability of the nucleation core of MVs by simply using a PS-enriched Langmuir monolayer. We show that PS-enrichment at membranes creates domains for local increase of supersaturation, leading to the nucleation of ACP at the interface though a multistep process.

2. Materials and methods

Isolation of MVs from femurs of chicken embryos

The protocol used for the extraction of MVs used a collagenase digestion step (Buchet et al., 2013). Briefly, 20 chicken embryos (17 days after fertilization) were sacrificed by decapitation. The femurs were dissected and slices (1–3 mm thick) of the epiphyses/growth plates finely cut and digested for 3 h, at 37°C, in synthetic cartilage buffer (SCL) buffer supplemented with 1 mM $CaCl_2$ and type I collagenase (Sigma, from *Clostridium histolyticum*) at concentration of 300 U/g of tissue. After digestion, the suspension was filtered through a nylon membrane (100 μm). The supernatant was centrifuged at 600 g to collect all released cell material. The MVs were purified by consecutive centrifugations at 20,000 g for 30 min and 80,000 g for 1 h, both at 4°C. The final pellet was homogenized in 200 μL of SCL, which is a buffer that mimic the native environment of MVs in the cartilage, and stored at 4°C(Wu et al., 1997). SCL is composed of 1.42 mM NaH_2PO_4, 1.83 mM $NaHCO_3$, 12.7 mM KCl, 0.57 mM $MgCl_2$, 5.55 mM D-glucose, 63.5 mM saccharose, 16.5 mM Tris (2-Amino-2-hydroxymethyl-propane-1,3-diol), 100 mM NaCl, 0.7 mM Na_2SO_4 in water at pH 7.6. All procedures involved in the euthanasia of animals were approved by the ethics committee of FFCLRP protocol 19.1.842.59.13.

Characterization of isolated MVs

Alkaline phosphatase (ALP) activity was determined by the hydrolysis of *p*-nitrophenyl phosphate (p-NPP, Sigma-Aldrich) in a reaction medium containing 10 mM p-NPP and 1 mM $MgCl_2$ in AMPOL buffer (2-amino-2-methyl-1-propanol), pH 10.3, at 37°C. The reaction was monitored by changes in the absorbance at 405 nm related to the formation of the yellowish product p-nitrophenolate $(p\text{-}NP)^-$ and the specific activity expressed as μmol pNP^-/min/mg of protein. The total protein content was determined by Hartree methodology (Hartree, 1972). The protein profile of MVs was evaluated by SDS-PAGE electrophoresis using 10 % polyacrylamide gel and stained with silver nitrate. The size of the MVs in SCL was evaluated by Dynamic Light Scattering (DLS) (Zeta Sizer Nano ZS, Malvern). The morphology of the MVs was evaluated by Atomic Force Microscopy (AFM) (Shimadzu SPM-9600). MVs (0.5 μg/mL) in SCL were fixed with 1% (v/v) glutaraldehyde and the suspension dropped in a freshly-cleaved mica plate, dried under ambient temperature and analyzed by AFM using dynamic mode, as detailed described in (Bolean et al., 2017).

The mineralization of MVs was evaluated in SCL supplemented with 2 mM Ca^{2+} and 3.42 mM NaH_2PO_4, at 37°C. The concentration of MVs in the medium was standardized at 20 μg of protein/mL. After 24 h, the samples were centrifuged, dripped on a carbon-coated copper grid, and analyzed by TEM (JEM-2100-JEOL).

Extraction of the lipid fraction from MVs

The lipid fraction of the MVs was obtained from the protocol developed by Abdallah et al. (Abdallah et al., 2014). Briefly, 100 μL of the MV suspension was mixed with 400 μL of methanol:chloroform (2:1 ratio), and shaken vigorously for 1 min, and then incubated at room temperature for 30 min. Chloroform and water were subsequently added to the supernatant. The phase separation was performed by centrifugation at 2,000 g for 10 min. The chloroform phase containing the lipid fraction of the MVs was then collected and used immediately for analysis.

Langmuir monolayers and surface pressure (π) vs area (A) isotherms

1,2-dipalmitoyl-sn-glycero-3-phosphatidylcholine (DPPC; purity > 99%, Avanti Lipids) and 1,2-dipalmitoyl-sn-glycero-3-phospho-L-serine (DPPS; > 99%; Avanti Lipids) or the lipid extract from MVs were used to build the Langmuir monolayers, using a Langmuir trough (Insight Brazil, 216 cm^2). Monolayers were obtained after spreading the lipids solubilized in chloroform:methanol (3:1 ratio) on a subphase containing either ultrapure water (surface tension of 72.3 mN m^{-1} and conductivity 1.1 μS cm^{-1}, at 25°C) or the solution of interest. After spreading the lipid solution, the monolayer was compressed at a rate of 0.42 mm^2 s^{-1} with a constant temperature of 25 ± 1°C and the π changes were acquired using a Wilhelmy plate, to construct the π-A isotherms.

The isothermal compressibility C_s^{-1} of the monolayers was calculated from the slope of the π-A isotherm in a given value of area occupied by molecule (A), according to the equation 1. The condensation state of the monolayer was identified from the values of C_s^{-1} at a given π according to (Davies and Rideal, 1963). Liquid-expanded (LE) state of the monolayer is characterized by C_s^{-1} values ranging from 12 to 50 mN/m, liquid-condensed states (LC) from 100 to 250 mN/m and solid state from values higher than 1000 mN/m.

$$C_s^{-1} = -A\left(\frac{\partial \pi}{\partial A}\right)_T \quad (1)$$

The Gibbs free energy of excess, ΔG_{exc}, for the DPPC:DPPS (8:2) mixture was calculated from the integration of the π - A isotherms of the mixed monolayer and the monolayers of the pure components, according to the equation 2,

$$\Delta G_{exc} = \int_o^{\pi} (A_{12} - (x_1 A_1 + x_2 A_2) d\pi \quad (2)$$

where A_{12} is the area occupied by the molecule in the mixture of components 1 and 2.

In situ mineralization of Langmuir monolayers

Mineralization of the Langmuir monolayers was carried out with a modified SCL buffer (m-SCL) composed by 10.0 mM 2-[4-(2-hydroxyethyl)piperazin-1-yl]ethanesulfonic acid (HEPES), 5.13 mM Na_2HPO_4, 1.83 mM $NaHCO_3$, 12.7 mM KCl, 0.57 mM $MgCl_2$, 3.0 mM $CaCl_2$, 100 mM NaCl, 0.7 mM Na_2SO_4. The pH of solution was adjusted to 7.4 and promptly used for the experiments. All experiments were performed at 25°C and π kept constant at 30 mN/m simulating the lipid organization in cells (Blume, 1979). During the experiment, aliquots were collected from the subphase below the movable barrier for subsequent potentiometric measurement of the concentration of free Ca^{2+} ($[Ca^{2+}]_{free}$) using an ion-selective electrode (Bante Instruments, Shanghai, China) using a Bante320 multiparameter meter.

Phase-modulated infrared absorption spectroscopy (PM-IRRAS) of mineralizing monolayers was performed *in situ* in the Langmuir trough, at π = 30 mN/m, in the 800–4000 cm^{-1} range, with a resolution of 8 cm^{-1} using a KSV PMI550 spectrophotometer (KSV Instruments) coupled to a polarizer modulator PEM100. The incidence angle was 81°. The spectra are presented as a function of the PM-IRRAS signal, obtained from the equation $S = \Delta R / R = (Rp - Rs) / (Rp + Rs)$, where Rp and Rs are the reflectance obtained from the incident beam polarized parallel (s) or perpendicular (p) to the plane of incidence. The PM-IRRAS signal is presented as $\Delta S = (S - S_0) / S_0$, where S is the response obtained for the subphase covered with the Langmuir monolayer and S_0 is the response obtained for the pure subphase. The changes in morphology of the monolayers due to mineralization as a function of time was investigated by TEM (JEM-2100-JEOL microscope) through the transfer of the monolayers to carbon-coated copper grids. After 240 min of mineralization, the material formed at the air-liquid interface was collected and immediately analyzed by Fourier-transform infrared spectroscopy (FTIR) coupled with an attenuated total reflectance (ATR) accessory (Shimadzu-IRPrestige-21).

The surface zeta-potential (ζ) of the samples was measured in a surface ζ-potential cell (ZEN 1020) hyphened to a Zetasizer Nano ZS (Malvern Instruments). Mobility of the tracer particles (polystyrene nanospheres – Duke Scientific Corporation, 200 nm, $\zeta = -54.6 \pm 7.04$ mV in pure water) in the vicinity of the charged test surface mounted on a dip cell was measured by phase analysis light scattering and a simple model used to describe the electroosmotic flow near the fitted surface [30]. To this, Y-type LB film bilayers were transferred to silicon samples equal or smaller than 7 mm × 4 mm and with thickness of 1 mm, maintaining the surface pressure constant at 30 mN m^{-1}. After the transference, the samples were immersed in the m-SCL for different periods. The sample holder was carefully mounted in liquid medium to avoid LB film disruption. Measurements were repeated at least three times at 25°C.

Results

Isolation and characterization of MVs

Collagenase-released MVs presented spherical shape and average diameter of 200 nm (Fig. 1a–b). The purity was confirmed by SDS-PAGE, which indicated their characteristic bands

(Supplementary Figure S1a–b)(Wuthier and Lipscomb, 2011). DLS measurements attested the size distribution of MV centered at 200 nm (Supplementary Figure S1c) as described in the literature for these class of vesicles (Zhang et al., 2005). The extract containing the MVs exhibited higher ALP activity when compared to cell lysate (Fig. 1c). Increased ALP activity is an intrinsic characteristic and a marker of MVs functionality (Anderson, 1995). To verify the function of MVs, the ability of these structures to mineralize was determined. Incubation of MVs in SCL supplemented with 2 mM $CaCl_2$ and 3.42 mM NaH_2PO_4 leaded to an increase in the turbidity of the dispersion within 3 h (Supplementary Figure S1d) that was associated to the beginning of mineralization by association of Ca^{2+} and Pi inside the vesicles (Plaut et al., 2019). Although SCL is a supersaturated solution regarding the most important biominerals (see Supplementary Table S1), it does not induce a significant mineralization by itself as probed by turbidity (Supplementary Figure S1), attesting that MVs are essential to initiate mineralization. TEM images (Figure 1d–e) show the presence of spherical structures with regions of higher contrast after 24 h of incubation in the mineralizing medium, confirming the formation of mineral by the MVs. There was a heterogeneous population of vesicles in terms of mineralization degree as suggested by their different contrasts (blue arrow, Fig. 1d). Although it was not possible to conclude on the location of the mineral phase by the TEM images, dark edges in some vesicles (red arrow, Fig. 1d) indicated that mineral formation was membrane-driven, in accordance with AFM of MVs under hydrated conditions (Plaut et al., 2019). The absence of rings in the electron diffraction pattern of the mineralized structures indicated the precipitation of amorphous material and elemental analysis by EDS (Fig. 1e) attested to the presence of Ca and P (Ca/P ratio = 1.0), typical of ACP.

Langmuir monolayers mimicking MVs lipidic composition

Langmuir monolayers of selected lipid compositions allowed us to obtain thermodynamic parameters to investigate the effect of specific lipids on nucleation ability of MVs. Monolayers were built in a subphase containing the supersaturated solution m-SCL, at 25°C (composition of m-SCL is described in Supplementary Table S1). Firstly, monolayers composed of DPPC and DPPS (Fig. 2) and the mixture (DPPC:DPPS 8:2, molar ratio) in a proportion similar to the one found in MVs was studied. The features of DPPC and DPPS isotherms (Fig. 2a), recorded at 25°C in subphase containing the m-SCL solution, were in accordance with previous reports (Chen et al., 2010; Ma and Allen, 2006). DPPC isotherm (Fig. 2a, black line) exhibited an onset molecular area at 100 $Å^2$, corresponding to the beginning of the liquid-expanded (LE) phase, and a plateau at $\pi \sim 10$ mN m^{-1} in the range of 65–80 $Å^2$, corresponding to LC-LE phase coexistence region. The increase of π after this plateau is assigned to the formation of pure LC phase. The phase transitions were also demonstrated by changes in the C_s^{-1} values of the monolayers (Fig. 2-inset). Static surface elasticity values (C_s^{-1}) are a measurement of the tendency of the monolayers to resist to the compression at a given π, translating also into the packing state of the monolayer. Higher C_s^{-1} values indicates more compact monolayer. DPPS isotherm (Fig. 2, blue line) exhibited an onset molecular area at 55 $Å^2$ and a better packing, revealed by the displacement to smaller mean molecular area, compared to pure DPPC monolayers. This was assigned to the smaller size of the serine group present on DPPS polar head compared to the choline group present at DPPC. Compact monolayers are a characteristic feature of phospholipids with

small polar heads, e.g. DPPS, which facilitate strong van der Waals interactions between the nonpolar tails, in addition to the possibility of hydrogen bonds with the subphase (Hauser et al., 1981). The absence of phase-coexistence region is also a characteristic of DPPS isotherms. The mixed DPPC:DPPS (8:2) (Fig. 2, red line) resembles the pure-DPPC isotherm with a slight expansion to higher molecular areas at condensed states. This might indicate repulsive interactions between the phospholipid molecules in the mixture. Indeed, calculation of the ΔG_{ex} for the DPPC:DPPS (8:2) mixture attested the formation of a non-ideal mixture ($\Delta G_{ex} > 0$) and the predominance of non-favored interactions between the lipid molecules in the mixed monolayer over the pure ones (Supplementary Figure S3). At π= 30 mN/m, the pure DPPC, DPPC:DPPS (8:2), and pure DPPS monolayers displayed C_s^{-1} values higher than 200 mN/m, indicating that molecules are assembled in a LC state that resembles the lipid packing found in the liquid-ordered phases dispersed in a liquid-disordered matrix in biological membrane (Vollhardt and Fainerman, 2006). Therefore, 30 mN/m was the π chosen value for the mineralization experiments.

Mineralization induced on Langmuir monolayers composed by lipids of selected compositions

DPPS monolayers efficiently induces mineral formation within 240 min of reaction, as shown in Fig. 3. To attest localized mineral formation at the air-liquid interface, changes in the chemical composition of the DPPS monolayer along the mineralization experiment was followed by PM-IRRAS (Fig. 3a). This infrared spectroscopy technique is sensible to the presence and orientation of chemical groups at the air-liquid interface (Volpati et al., 2014), and identify events occurring restricted to the interface. As shown in the PM-IRRAS spectrum of the DPPS monolayer (Fig. 3a), longer is the reaction time, greater are the changes in the spectral region of 1150–950 cm^{-1}. At this spectral range, it is expected to observe absorptions from the ν_3 and ν_1 domains of the PO_4^{3-} group in the growing mineral phase (Rey et al., 2014). However, other bands related to absorptions from chemical groups of the phospholipids can also be found in this range (see Supplementary Table S2). The intensity of the band at 1020–1040 cm^{-1} ascribed to the absorption of the ν_3 of PO_4 groups in calcium phosphates (marked by the blue box in Fig. 3a) increased after 180 minutes, indicating the formation of Ca-phosphate species at the interface. This result corroborates previous investigations conducted experimentally (Habraken et al., 2013) and by molecular dynamics (Lin and Chiu, 2017) showing that Ca-phosphate species typically absorb in this infrared region. Formation of ACP at the DPPS monolayer after 240 min of mineralization was evidenced by FTIR spectrum of the material collected from the air-liquid interface (Fig. 3b). A broad band centered at 1030 cm^{-1} (ν_3 PO_4) with a small shoulder at 950 cm^{-1} (ν_1) are spectral characteristics of ACP formation(Rey et al., 2014). TEM images of the DPPS monolayer after 240 min of reaction shows particles with high contrast forming a homogenous film (Fig. 3c). SAED confirmed the formation of amorphous structures (Fig. 3c-insert).

Changes in the $[Ca^{2+}]_{free}$ in the subphase measured *in-situ* along mineralization in the presence of the DPPS monolayer gave insight into the multistep process occurring at the interface (Fig. 3d). Within the first 60 min, no significant changes in the $[Ca^{2+}]_{free}$ was observed. However, from this time on, it was observed a decrease in the $[Ca^{2+}]_{free}$,

indicating the consumption of Ca^{2+} from the subphase to form the ACP at the interface mediated by PS polar heads. Measurements of DPPS bilayer surface ζ-potential revealed a decrease of the negative surface charge along the mineralization (Fig. 3e). Ca^{2+} interacts with DPPS polar heads (Melcrová et al., 2016) as confirmed by the decrease in the ζ-potential of the DPPS bilayer in presence of Ca^{2+}. The DPPS bilayers induced the stabilization of calcium-phosphate complexes that specifically interacts with the lipid headgroup in the calcium phosphate supersaturated solution. The coalescence of these complexes leads to the formation of ACP as indicated by a “more electroneutral” interface after 240 min.

In order to access the ability of DPPS to stabilize ion complexes with the Ca^{2+} and phosphate ions to trigger the ACP nucleation, we performed a titration experiment to infer about chemical speciation in solution during pre-nucleation stages (Supplementary Figure S3). By using the approach developed by (Habraken et al., 2013), a Ca^{2+} stock solution was slowly titrated to a phosphate solution in presence of phosphoserine, a water-soluble mimetic of the DPPS headgroup, as additive. In this experiment, we evaluate changes in the $[Ca^{2+}]_{free}$ regarded to the addition of Ca^{2+} ($[Ca^{2+}]_{add}$) to the solution. Therefore, information about the equilibrium between bonded and free ions in solution was accessed. One import step during this crystallization experiment is the pre-nucleation stage, i.e. a linear range in the $[Ca^{2+}]_{free}$ *versus* $[Ca^{2+}]_{add}$ curve before any bulk precipitation is observed. This stage is marked by an equilibrium between soluble association complexes between Ca^{2+} and phosphate ions. In presence of phosphoserine, we observed a change in the slope of the prenucleation stage (Fig.S3-inset) due to changes in how the solution is assimilating Ca^{2+}, which denote specific association between the ions and the charged PS group. This evidences the ability of PS to induce specific associations with Ca^{2+} and phosphate ions that leads to the ACP nucleation.

In native MVs, PS molecules are dispersed in a lipid membrane, therefore the next step was to evaluate the effect on mineralization by DPPS molecules diluted in a DPPC monolayer, mimicking a native-like lipid composition. Unlike in DPPS monolayer, the structures formed on DPPC:DPPS (8:2, molar ratio) monolayer are heterogeneously distributed along the surface (Fig. 4). Spherical structures of ~ 5 nm with amorphous SAED pattern are observed forming the micrometric aggregates. After 12 h, this amorphous phase crystallizes (as shown by the presence of diffraction rings in the SAED patterns), forming platelets homogeneously distributed along the monolayer. This morphology is characteristic of biomimetic apatite (Habraken et al., 2013; Hentrich et al., 2017). After 24 h, these structures grow leading to the monolayer rupture and formation of crystalline agglomerates with micrometric dimensions.

DPPC monolayers did not induce mineral formation within 240 min. This was evidenced by no significant changes in the PM-IRRAS spectra of the monolayer along 240 min of reaction (Supplementary Figure S4). Monolayers composed of pure DPPC did not promote formation of mineralized structures after 240 min, as shown by TEM images (Supplementary Figure S5). Moreover, absence of mineralization in the pure DPPC monolayer was corroborated by analysis of the rheological behavior of the monolayers upon mineralization (Supplementary Figure S6). Rheological properties of the monolayer are dependent on the dynamic packing

behavior of molecules (Rodrigues et al., 2018). DPPS monolayers had higher viscoelastic components compared to DPPC monolayer during the mineralization experiment. After 60 min, the viscoelastic component of the complex rheological behavior values (G") for the DPPC monolayer was 29 mN/m, while it was 87 mN/m for the DPPS monolayer. The growing mineral phase on the DPPS monolayer enhanced the viscous effect to the elasticity of the monolayer in a such way that enabled any compression/decompression cycles after 3 h. This was in contrast with the pure DPPC monolayer, where it was possible to monitor compression/decompression cycles. This is a macroscopic evidence of the dense mineralization of the DPPS monolayer in a short time period. It is worth to highlight that it is not a conclusion that DPPC monolayers are not able to mediate calcium phosphate nucleation at all. Indeed, several papers in the literature describes DPPC membranes as organic templates for heterogeneous calcium phosphate growth (Ruiz et al., 2017; Zhang et al., 2004). However, in the experimental conditions and time frame herein used, it is remarkable that DPPS monolayers induce faster mineralization than pure DPPC.

Mineralization induced on Langmuir monolayer composed by the lipid extract of MVs

To further explore mineral formation in a native-like lipid environment, the ability to induce mineral formation on monolayers formed by the lipid fraction extracted from MVs was evaluated. The lipid fraction extracted from the MVs forms an expanded monolayer that reaches the LC state (C_s^{-1} > 100 mN/m) at π close to 30 mN/m (Supplementary Figure S7), which is the surface pressure where the mineralization was evaluated. High expanded monolayers are expected for monolayers composed by biological extracts due to presence of non-identical lipids with different levels of unsaturation. PM-IRRAS of MV-lipid extracts changed with the incubation time in the 1100–950 cm^{-1} region (Fig. 5a), characteristic of calcium phosphate absorption bands. This suggests the formation of calcium phosphate complexes that enabled the nucleation of ACP at the interface.

TEM images of the monolayers transferred after 240 min (Fig. 5b) revealed the presence of nanometric particles that aggregated into bigger structures (red arrow). It is worth to notice the similarity between the mineral structures observed on the monolayer of the MV-lipid extract (Fig. 5b) and the ones observed on the mixed DPPC:DPPS monolayer (Fig. 4b). The nucleation points emerged on the monolayer leading to the aggregation of nanometric structures into larger ones. It is now perceivable that the lipids in MVs had the ability to induce mineral formation. This ability can be mimetized by a simple monolayer composed by a DPPS-enriched monolayer, recreating *in vitro* the ability of the nucleation core of MVs to induce mineral formation.

3. Discussion

Altogether, our findings suggest a multistep crystallization pathway for calcium phosphate formation within the MVs mediated by the PS-enriched nucleation core. Calcium phosphate nucleation was fastly induced on DPPS-enriched monolayers. Since no mineralization was observed in pure DPPC monolayers, it is notable that PS-enrichment is the driven force to trigger mineral nucleation, recreating *in vitro*, in conditions of membrane-like structure, the nucleation ability of the nucleation core of MVs.

Accumulation of phosphate and Ca^{2+} under charged monolayers has been promptly observed in supersaturated solutions (Uysal et al., 2013). However, the simple addition and accumulation of the ionic species at the interface is not enough to promote mineral phase formation, being necessary to decrease an energetic barrier to the nucleation of the first nuclei (Garcia et al., 2019; Mancardi et al., 2017; Yang et al., 2019). To fulfill this task, the role of the organic matrix in the nucleation of calcium phosphates comes into play. Highly charged species act to stabilize calcium phosphate complexes (Yang et al., 2019), as extensively studied for non-collagenous proteins and their charged polymers analogues (e.g. polyaspartic acid). Zhao (Zhao et al., 2018) recently showed that osteocalcin bears highly charged amino acid residues in a specific arrangement that helps the stabilization of calcium phosphate complexes, energetically favoring their growth towards the formation of ACP. Herein, we show that PS is able to stabilize pre-nucleation complexes prior to ACP formation, mainly due to specific and favorable association between charged groups in DPPS polar head and precursor ions from the solution. The ability to form energetic favorable complexes between PS and surrounding Ca^{2+} and phosphate ions has been also proposed by other authors (Kesseli et al., 2020; Taylor et al., 1998; Wu et al., 2008). Therefore, we revisited the studies from Wuthier's group on the mineralization ability of the nucleation core by proposing that specific arrangements between PS headgroups creates metastable states that favor ACP formation within MVs. This multistep process goes in accordance with the currently accepted mechanism for the formation of calcium phosphates in biological media: the apatite formation occurs from an amorphous phase, which is the result of the aggregation of calcium phosphate complexes(Dey et al., 2010; Habraken et al., 2013; Mahamid et al., 2011a).

The existence of a PS-enriched nucleation core in the MVs can also be analyzed from a thermodynamic point-of-view. The nucleation of the monolayer composed by the DPPC:DPPS mixture, observed in Fig. 4, started by discreet dots distributed along the interface, that aggregated into bigger assemblies. The ΔG_{exc} value found for mixed DPPC:DPPS monolayer 8:2 (molar ratio) was +130 J/mol in the conditions in this study, at π=30 mN/m. Positive values for ΔG_{exc} can be understood as the driving force that directs the formation of lipid domains (Almeida, 2009) and has been described in the literature for PC:PS mixtures (Boettcher et al., 2011; Ross et al., 2001). Thus, clustering of PS molecules in the MVs is the origin of the nucleation core. PS-enriched nanometric domains within the MVs membrane create local sites where ACP nucleation is favored. *In vivo*, this mechanism of PS-rich nanodomains formation may also have the participation of proteins. (Faiß et al., 2008) demonstrated that the presence of annexin promotes intensification in the formation of PS-rich nanodomains in lipid bilayers composed of PC/PS. Indeed, isolation of nucleation core of MVs revealed the presence of annexins strongly bound to the PS-calcium phosphate complexes extracted from native MVs(Wu et al., 1997). Therefore, it cannot be excluded that mineral nucleation in MVs could also have the participation of other molecules different than PS. Moreover, the origin of the nucleation core in the MVs, i.e., if it is formed before or after their biogenesis is still an enigma to be unveiled in future studies.

Finally, the key function of PS in initiating mineralization is underlined by mutations of phosphatidylserine synthase-1 responsible for the synthesis of PS *in vivo,* causing excess bone density and bone malformations (Sousa et al., 2014). Indeed, *in vitro* gene silencing of

phosphatidylserine synthase-1 inhibited osteoblast differentiation and mineralization (Brum et al., 2017), attesting the major role that PS play on bone formation. This idea is elevated by an elegant characteristic of MVs: they are a compartmentalized environment where Ca^{2+} and phosphate ions accumulate, thus creating a local high supersaturation to nucleate ACP mediated by PS-rich nanometric domains, the so-called nucleation core of MVs. We can summarize the ideas of how PS-mineral complexes might be involved in the bone mineralization in the scheme presented in the Fig. 6.

4. Conclusions

DPPS-enriched Langmuir monolayers were suitable models to mimic the inner leaflet of MVs to initiate mineralization. This was consistent with PS being the major entity responsible for the biomineral nucleation ability of MVs (Wu et al., 2008). The mineralization induced on DPPS-enriched monolayers was reproduced in a similarly manner on the monolayers composed by lipid-extract of MVs. Therefore, Langmuir monolayers were revealed as promising approach to determine lipid-lipid and lipid-protein interactions occurring during the mineralization induced by MVs. Association with other advanced characterization methods not used herein (e.g., cryo-TEM morphological analysis and *in-situ* fluorescence and X-ray scattering/diffraction techniques) opens a window to future studies using Langmuir monolayers to delineate molecular mechanisms of bone biomineralization. Finally, our findings suggest the possibility of PS playing a major role during ossification, making provision for future studies in order to unveil the origin of the biomineral precursor phase.

Supplementary Material

Refer to Web version on PubMed Central for supplementary material.

Acknowledgments

We would like to thank the Fundação de Amparo à Pesquisa do Estado de São Paulo (17/20846-2, 14/24249-0, 2016/21236-6, 2017/08892-9), Coordenação de Aperfeiçoamento de Pessoal de Nível Superior - Brasil (CAPES) (Finance Code 001, #88887.320304/2019-00), and Conselho Nacional de Desenvolvimento Científico e Tecnológico (CNPq) (304021/2017-2) for the financial support given to our laboratory. MAEC and CT received FAPESP grant. M. Bolean received CAPES grant. APR, LC and PC are CNPq researchers. This work was also supported in part by grant DE12889 from the National Institutes of Health (USA) and Brazil-France USP-COFECUB Uc Sv 184/20 grant.

6. References

Abdallah D, Hamade E, Merhi RA, Bassam B, Buchet R, Mebarek S, 2014. Fatty acid composition in matrix vesicles and in microvilli from femurs of chicken embryos revealed selective recruitment of fatty acids. Biochem. Biophys. Res. Commun446, 1161–1164. 10.1016/j.bbrc.2014.03.069 [PubMed: 24685481]

Almeida PFF, 2009. Thermodynamics of lipid interactions in complex bilayers. Biochim. Biophys. Acta - Biomembr1788, 72–85. 10.1016/j.bbamem.2008.08.007

Anderson HC, 1995. Molecular Biology of Matrix Vesicles. Clin Orthop Relat Res314, 266–80.

Anderson HC, 1967. Electron microscopic studies of induced cartilage development and calcification. J. Cell Biol35, 81–101. 10.1083/jcb.35.1.81 [PubMed: 6061727]

Anderson HC, Sipe JB, Hessle L, Dhamyamraju R, Atti E, Camacho NP, Millán JL, 2004. Impaired Calcification Around Matrix Vesicles of Growth Plate and Bone in Alkaline Phosphatase-Deficient Mice. Am. J. Pathol164, 841–847. 10.1016/S0002-9440(10)63172-0 [PubMed: 14982838]

Anghileri LJ, Dermietzel R, 1973. Calcium-phosphate-phospholipid complexes in experimental tumors: their possible relationship with tumor calcification. Zeitschrift für Krebsforsch. und Klin. Onkol79, 148–156. 10.1007/BF00303672

Beck L, 2019. Expression and function of Slc34 sodium–phosphate co-transporters in skeleton and teeth. Pflugers Arch. Eur. J. Physiol471, 175–184. 10.1007/s00424-018-2240-y [PubMed: 30511265]

Blume A, 1979. A comparative study of the phase transitions of phospholipid bilayers and monolayers. Biochim. Biophys. Acta - Biomembr557, 32–44. 10.1016/0005-2736(79)90087-7

Boettcher JM, Davis-Harrison RL, Clay MC, Nieuwkoop AJ, Ohkubo YZ, Tajkhorshid E, Morrissey JH, Rienstra CM, 2011. Atomic View of Calcium-Induced Clustering of Phosphatidylserine in Mixed Lipid Bilayers. Biochemistry50, 2264–2273. 10.1021/bi1013694 [PubMed: 21294564]

Bolean M, Borin IA, Simão AMS, Bottini M, Bagatolli LA, Hoylaerts MF, Millán JL, Ciancaglini P, 2017. Topographic analysis by atomic force microscopy of proteoliposomes matrix vesicle mimetics harboring TNAP and AnxA5. Biochim. Biophys. Acta - Biomembr1859, 1911–1920. 10.1016/j.bbamem.2017.05.010 [PubMed: 28549727]

Bolean M, Izzi B, van kerckhoven S, Bottini M, Ramos AP, Millán JL, Hoylaerts MF, Ciancaglini P, 2020. Matrix vesicle biomimetics harboring Annexin A5 and alkaline phosphatase bind to the native collagen matrix produced by mineralizing vascular smooth muscle cells. Biochim. Biophys. Acta - Gen. Subj1864, 129629. 10.1016/j.bbagen.2020.129629 [PubMed: 32360152]

Bolean M, Simão AM., Favarin BZ, Millán JL, Ciancaglini P, 2010. The effect of cholesterol on the reconstitution of alkaline phosphatase into liposomes. Biophys. Chem152, 74–79. 10.1016/j.bpc.2010.08.002 [PubMed: 20810204]

Bolean M, Simão AMS, Kiffer-Moreira T, Hoylaerts MF, Millán JL, Itri R, Ciancaglini P, 2015. Proteoliposomes with the ability to transport Ca2+ into the vesicles and hydrolyze phosphosubstrates on their surface. Arch. Biochem. Biophys584, 79–89. 10.1016/j.abb.2015.08.018 [PubMed: 26325078]

Bonucci E, 1967. Fine structure of early cartilage calcification. J. Ultrastruct. Res20, 33–50. 10.1016/S0022-5320(67)80034-0 [PubMed: 4195919]

Boonrungsiman S, Gentleman E, Carzaniga R, Evans ND, McComb DW, Porter AE, Stevens MM, 2012. The role of intracellular calcium phosphate in osteoblast-mediated bone apatite formation. Proc. Natl. Acad. Sci109, 14170–14175. 10.1073/pnas.1208916109 [PubMed: 22879397]

Boskey AL, Posner AS, 1975. Extraction of a calcium-phospholipid-phosphate complex from bone. Calcif. Tissue Res19, 273–283. 10.1007/BF02564010

Bottini M, Mebarek S, Anderson KL, Strzelecka-Kiliszek A, Bozycki L, Simão AMS, Bolean M, Ciancaglini P, Pikula JB, Pikula S, Magne D, Volkmann N, Hanein D, Millán JL, Buchet R, 2018. Matrix vesicles from chondrocytes and osteoblasts: Their biogenesis, properties, functions and biomimetic models. Biochim. Biophys. Acta - Gen. Subj1862, 532–546. 10.1016/j.bbagen.2017.11.005 [PubMed: 29108957]

Brum AM, van der Leije CS, Schreuders-Koedam M, Verhoeven J, Janssen M, Dekkers DH, Demmers JA, Eijken M, van de Peppel J, van Leeuwen JP, van der Eerden BC, 2017. Identification of Chloride Intracellular Channel Protein 3 as a Novel Gene Affecting Human Bone Formation. JBMR Plus1, 16–26. 10.1002/jbm4.10003 [PubMed: 30283877]

Buchet R, Pikula S, Magne D, Mebarek S, 2013. Isolation and Characteristics of Matrix Vesicles, in: Phosphatase Modulators. pp. 115–124. 10.1007/978-1-62703-562-0_7

Caseli L, Nobre TM, Ramos AP, Monteiro DS, Zaniquelli MED, 2015. The Role of Langmuir Monolayers To Understand Biological Events, in: Recent Progress in Colloid and Surface Chemistry with Biological Applications. pp. 65–88. 10.1021/bk-2015-1215.ch004

Chen X, Huang Z, Hua W, Castada H, Allen HC, 2010. Reorganization and Caging of DPPC, DPPE, DPPG, and DPPS Monolayers Caused by Dimethylsulfoxide Observed Using Brewster Angle Microscopy. Langmuir26, 18902–18908. 10.1021/la102842a [PubMed: 21086993]

Cotmore JM, Nichols G, Wuthier RE, 1971. Phospholipid-calcium phosphate complex: Enhanced calcium migration in the presence of phosphate. Science (80-.). 172, 1339–1341. 10.1126/science.172.3990.1339

Davies JT, Rideal EK, 1963. Interfacial Phenomena.

Derradi R, Bolean M, Simão AMS, Caseli L, Millán JL, Bottini M, Ciancaglini P, Ramos AP, 2019. Cholesterol Regulates the Incorporation and Catalytic Activity of Tissue-Nonspecific Alkaline Phosphatase in DPPC Monolayers. Langmuir35, 15232–15241. 10.1021/acs.langmuir.9b02590 [PubMed: 31702926]

Dey A, Bomans PH, Muller FA, Will J, Frederik PM, de With G, Sommerdijk NA, 2010. The role of prenucleation clusters in surface-induced calcium phosphate crystallization. Nat. Mater9, 1010–1014. 10.1038/nmat2900 [PubMed: 21076415]

Dillon S, Staines KA, Millán JL, Farquharson C, 2019. How To Build a Bone: PHOSPHO1, Biomineralization, and Beyond. JBMR Plus3, e10202. 10.1002/jbm4.10202 [PubMed: 31372594]

Faiß S, Kastl K, Janshoff A, Steinem C, 2008. Formation of irreversibly bound annexin A1 protein domains on POPC/POPS solid supported membranes. Biochim. Biophys. Acta - Biomembr1778, 1601–1610. 10.1016/j.bbamem.2008.01.003

Favarin BZ, Bolean M, Ramos AP, Magrini A, Rosato N, Millán JL, Bottini M, Costa-Filho AJ, Ciancaglini P, 2020. Lipid composition modulates ATP hydrolysis and calcium phosphate mineral propagation by TNAP-harboring proteoliposomes. Arch. Biochem. Biophys108482. 10.1016/j.abb.2020.108482 [PubMed: 32710882]

Garcia NA, Malini RI, Freeman CL, Demichelis R, Raiteri P, Sommerdijk NAJM, Harding JH, Gale JD, 2019. Simulation of Calcium Phosphate Prenucleation Clusters in Aqueous Solution: Association beyond Ion Pairing. Cryst. Growth Des19, 6422–6430. 10.1021/acs.cgd.9b00889

Genge BR, Wu LNY, Wuthier RE, 2007. In vitro modeling of matrix vesicle nucleation: Synergistic stimulation of mineral formation by annexin A5 and phosphatidylserine. J. Biol. Chem282, 26035–26045. 10.1074/jbc.M701057200 [PubMed: 17613532]

Habraken WJEM, Tao J, Brylka LJ, Friedrich H, Bertinetti L, Schenk AS, Verch A, Dmitrovic V, Bomans PHH, Frederik PM, Laven J, van der Schoot P, Aichmayer B, de With G, DeYoreo JJ, Sommerdijk NAJM, 2013. Ion-association complexes unite classical and non-classical theories for the biomimetic nucleation of calcium phosphate. Nat. Commun4, 1507. 10.1038/ncomms2490 [PubMed: 23422675]

Hartree EF, 1972. Determination of protein: A modification of the lowry method that gives a linear photometric response. Anal. Biochem48, 422–427. 10.1016/0003-2697(72)90094-2 [PubMed: 4115981]

Hauser H, Pascher I, Pearson RH, Sundell S, 1981. Preferred conformation and molecular packing of phosphatidylethanolamine and phosphatidylcholine. Biochim. Biophys. Acta - Rev. Biomembr650, 21–51. 10.1016/0304-4157(81)90007-1

Irving JT, Wuthier RE, 1968. Histochemistry and Biochemistry of Calcification With Special Reference to the Role of Lipids. Clin. Orthop. Relat. Res56, 237–260. [PubMed: 4172398]

Iwayama T, Okada T, Ueda T, Tomita K, Matsumoto S, Takedachi M, Wakisaka S, Noda T, Ogura T, Okano T, Fratzl P, Ogura T, Murakami S, 2019. Osteoblastic lysosome plays a central role in mineralization. Sci. Adv10, 1–10.

Jiao K, Niu LN, Ma CF, Huang XQ, Pei DD, Luo T, Huang Q, Chen JH, Tay FR, Wu LNYY, Genge BR, Wuthier RE, Boyan BD, Boskey AL, Posner AS, Cruz MAE, Ciancaglini P, Ramos AP, Boskey AL, Posner AS, Anghileri LJ, Dermietzel R, Wuthier RE, Shapiro IM, Shahlori R, Waterhouse GIN, Darwish TA, Nelson ARJ, McGillivray DJ, Bullough PG, Wu LNYY, Genge BR, Dunkelberger DG, LeGeros RZ, Concannon B, Wuthier RE, Skrtic D, Eanes ED, 1997. Physicochemical Characterization of the Nucleational Core of Matrix Vesicles. Calcif. Tissue Res19, 4404–4411. 10.1074/jbc.272.7.4404

Kerschnitzki M, Akiva A, Shoham A. Ben, Koifman N, Shimoni E, Rechav K, Arraf AA, Schultheiss TM, Talmon Y, Zelzer E, Weiner S, Addadi L, 2016. Transport of membrane-bound mineral particles in blood vessels during chicken embryonic bone development. Bone83, 65–72. 10.1016/j.bone.2015.10.009 [PubMed: 26481471]

Kesseli FP, Lauer CS, Baker I, Mirica KA, Van Citters DW, 2020. Identification of a calcium phosphoserine coordination network in an adhesive organo-apatitic bone cement system. Acta Biomater. 105, 280–289. 10.1016/j.actbio.2020.01.007 [PubMed: 31945507]

Lin TJ, Chiu CC, 2017. Structures and infrared spectra of calcium phosphate clusters by: Ab initio methods with implicit solvation models. Phys. Chem. Chem. Phys20, 345–356. 10.1039/c7cp05975b [PubMed: 29210384]

Lotsari A, Rajasekharan AK, Halvarsson M, Andersson M, 2018. Transformation of amorphous calcium phosphate to bone-like apatite. Nat. Commun9. 10.1038/s41467-018-06570-x

Ma G, Allen HC, 2006. DPPC Langmuir Monolayer at the Air−Water Interface: Probing the Tail and Head Groups by Vibrational Sum Frequency Generation Spectroscopy. Langmuir22, 5341–5349. 10.1021/la0535227 [PubMed: 16732662]

Mahamid J, Addadi L, Weiner S, 2011a. Crystallization Pathways in Bone92–97. 10.1159/000324229

Mahamid J, Aichmayer B, Shimoni E, Ziblat R, Li C, Siegel S, Paris O, Fratzl P, Weiner S, Addadi L, 2010. Mapping amorphous calcium phosphate transformation into crystalline mineral from the cell to the bone in zebrafish fin rays. Proc. Natl. Acad. Sci107, 6316–6321. 10.1073/pnas.0914218107 [PubMed: 20308589]

Mahamid J, Sharir A, Gur D, Zelzer E, Addadi L, Weiner S, 2011b. Bone mineralization proceeds through intracellular calcium phosphate loaded vesicles: a cryo-electron microscopy study. J. Struct. Biol174, 527–35. 10.1016/j.jsb.2011.03.014 [PubMed: 21440636]

Mancardi G, Hernandez Tamargo CE, Di Tommaso D, de Leeuw NH, 2017. Detection of Posner's clusters during calcium phosphate nucleation: a molecular dynamics study. J. Mater. Chem. B5, 7274–7284. 10.1039/C7TB01199G [PubMed: 32264177]

McLean FM, Keller PJ, Genge BR, Walters SA, Wuthier RE, 1987. Disposition of preformed mineral in matrix vesicles. Internal localization and association with alkaline phosphatase. J. Biol. Chem262, 10481–10488. [PubMed: 3611080]

Mebarek S, Abousalham A, Magne D, Do LD, Bandorowicz-Pikula J, Pikula S, Buchet R, 2013. Phospholipases of mineralization competent cells and matrix vesicles: Roles in physiological and pathological mineralizations. Int. J. Mol. Sci14, 5036–5129. 10.3390/ijms14035036 [PubMed: 23455471]

Melcrová A, Pokorna S, Pullanchery S, Kohagen M, Jurkiewicz P, Hof M, Jungwirth P, Cremer PS, Cwiklik L, 2016. The complex nature of calcium cation interactions with phospholipid bilayers. Sci. Rep6, 38035. 10.1038/srep38035 [PubMed: 27905555]

Millán JL, 2013. The role of phosphatases in the initiation of skeletal mineralization. Calcif. Tissue Int93, 299–306. 10.1007/s00223-012-9672-8 [PubMed: 23183786]

Nudelman F, Pieterse K, George A, Bomans PHH, Friedrich H, Brylka LJ, Hilbers PAJ, de With G, Sommerdijk NAJM, 2010. The role of collagen in bone apatite formation in the presence of hydroxyapatite nucleation inhibitors. Nat. Mater9, 1004–9. 10.1038/nmat2875 [PubMed: 20972429]

Pei D. dan, Sun J. long, Zhu C. hui, Tian F. cong, Jiao K, Anderson MR, Yiu C, Huang C, Jin C. xiong, Bergeron BE, Chen J. hua, Tay FR, Niu L. na, 2018. Contribution of Mitophagy to Cell-Mediated Mineralization: Revisiting a 50-Year-Old Conundrum. Adv. Sci5. 10.1002/advs.201800873

Plaut JS, Strzelecka-Kiliszek A, Bozycki L, Pikula S, Buchet R, Mebarek S, Chadli M, Bolean M, Simao AMS, Ciancaglini P, Magrini A, Rosato N, Magne D, Girard-Egrot A, Farquharson C, Esener SC, Millan JL, Bottini M, 2019. Quantitative atomic force microscopy provides new insight into matrix vesicle mineralization. Arch. Biochem. Biophys667, 14–21. 10.1016/j.abb.2019.04.003 [PubMed: 30998909]

Register TC, Mclean FM, Lows MG, Wuthier RE, 1986. Roles of Alkaline Phosphatase and Labile Internal Mineral in Matrix Vesicle-mediated Calcification. J. Biol. Chem261, 9354–9360. [PubMed: 3722200]

Rey C, Marsan O, Combes C, Drouet C, Grossin D, Sarda S, 2014. Characterization of Calcium Phosphates Using Vibrational Spectroscopies, in: Advances in Calcium Phosphate Biomaterials. pp. 229–266. 10.1007/978-3-642-53980-0_8

Reznikov N, Hoac B, Buss DJ, Addison WN, Barros NMT, McKee MD, 2020. Biological stenciling of mineralization in the skeleton: Local enzymatic removal of inhibitors in the extracellular matrix. Bone138, 115447. 10.1016/j.bone.2020.115447 [PubMed: 32454257]

Rodrigues RT, Morais PV, Nordi CSF, Schöning MJ, Siqueira JR, Caseli L, 2018. Carbon Nanotubes and Algal Polysaccharides To Enhance the Enzymatic Properties of Urease in Lipid Langmuir–Blodgett Films. Langmuir34, 3082–3093. 10.1021/acs.langmuir.7b04317 [PubMed: 29397738]

Ross M, Steinem C, Galla H-J, Janshoff A, 2001. Visualization of Chemical and Physical Properties of Calcium-Induced Domains in DPPC/DPPS Langmuir−Blodgett Layers. Langmuir17, 2437–2445. 10.1021/la001617x

Ruiz GCM, Cruz MAE, Faria AN, Zancanela DC, Ciancaglini P, Ramos AP, 2017. Biomimetic collagen/phospholipid coatings improve formation of hydroxyapatite nanoparticles on titanium. Mater. Sci. EngC77, 102–110. 10.1016/j.msec.2017.03.204

Simão AMS, Yadav MC, Narisawa S, Bolean M, Pizauro JM, Hoylaerts MF, Ciancaglini P, Millán JL, 2010. Proteoliposomes harboring alkaline phosphatase and nucleotide pyrophosphatase as matrix vesicle biomimetics. J. Biol. Chem285, 7598–7609. [PubMed: 20048161]

Sousa SB, Jenkins D, Chanudet E, Tasseva G, Ishida M, Anderson G, Docker J, Ryten M, Sa J, Saraiva JM, Barnicoat A, Scott R, Calder A, Wattanasirichaigoon D, Chrzanowska K, Simandlová M, Van Maldergem L, Stanier P, Beales PL, Vance JE, Moore GE, 2014. Gain-of-function mutations in the phosphatidylserine synthase 1 (PTDSS1) gene cause Lenz-Majewski syndrome. Nat. Genet46, 70–76. 10.1038/ng.2829 [PubMed: 24241535]

Taylor MG, Simkiss K, Simmons J, Wu LNY, Wuthier RE, 1998. Structural studies of a phosphatidyl serine-amorphous calcium phosphate complex. Cell. Mol. Life Sci54, 196–202. 10.1007/s000180050143 [PubMed: 9539964]

Uysal A, Stripe B, Lin B, Meron M, Dutta P, 2013. Assembly of amorphous clusters under floating monolayers: A comparison of in situ and ex situ techniques. Langmuir29, 14361–14368. 10.1021/la402682r [PubMed: 24164244]

Vollhardt D, Fainerman VB, 2006. Progress in characterization of Langmuir monolayers by consideration of compressibility. Adv. Colloid Interface Sci127, 83–97. 10.1016/j.cis.2006.11.006 [PubMed: 17208192]

Volpati D, Aoki PHB, Alessio P, Pavinatto FJ, Miranda PB, Constantino CJL, Oliveira ON, 2014. Vibrational spectroscopy for probing molecular-level interactions in organic films mimicking biointerfaces. Adv. Colloid Interface Sci207, 199–215. 10.1016/j.cis.2014.01.014 [PubMed: 24530000]

Wu LNY, Genge BR, Dunkelberger DG, LeGeros RZ, Concannon B, Wuthier RE, 1997. Physicochemical Characterization of the Nucleational Core of Matrix Vesicles. J. Biol. Chem272, 4404–4411. 10.1074/jbc.272.7.4404 [PubMed: 9020163]

Wu LNY, Genge BR, Kang MW, Arsenault AL, Wuthier RE, 2002. Changes in Phospholipid Extractability and Composition Accompany Mineralization of Chicken Growth Plate Cartilage Matrix Vesicles. J. Biol. Chem277, 5126–5133. 10.1074/jbc.M107899200 [PubMed: 11714705]

Wu LNY, Genge BR, Sauer GR, Wuthier RE, 1996. Characterization and Reconstitution of the Nucleational Complex Responsible for Mineral Formation by Growth Plate Cartilage Matrix Vesicles. Connect. Tissue Res35, 309–315. 10.3109/03008209609029205 [PubMed: 9084669]

Wu LNY, Genge BR, Wuthier RE, 2009. Differential effects of zinc and magnesium ions on mineralization activity of phosphatidylserine calcium phosphate complexes. J. Inorg. Biochem103, 948–962. 10.1016/j.jinorgbio.2009.04.004 [PubMed: 19477528]

Wu LNY, Genge BR, Wuthier RE, 2008. Analysis and molecular modeling of the formation, structure, and activity of the phosphatidylserine-calcium-phosphate complex associated with biomineralization. J. Biol. Chem283, 3827–3838. 10.1074/jbc.M707653200 [PubMed: 18077457]

Wuthier RE, 1971. Zonal analysis of phospholipids in the epiphyseal cartilage and bone of normal and rachitic chickens and pigs. Calcif. Tissue Res8, 36–53. 10.1007/BF02010121 [PubMed: 5135577]

Wuthier RE, 1969. A zonal analysis of inorganic and organic constituents of the epiphysis during endochondral calcification. Calcif. Tissue Res4, 20–38. 10.1007/BF02279103 [PubMed: 5344407]

Wuthier RE, Lipscomb GF, 2011. Matrix vesicles: structure, composition, formation and function in calcification. Front. Biosci. (Landmark Ed16, 2812–902. 10.1095/biolreprod.107.067082 [PubMed: 21622210]

Yang X, Wang M, Yang Y, Cui B, Xu Z, Yang X, 2019. Physical origin underlying the prenucleation-cluster-mediated nonclassical nucleation pathways for calcium phosphate. Phys. Chem. Chem. Phys21, 14530–14540. 10.1039/c9cp00919a [PubMed: 30984939]

Zhang L-J, Liu H-G, Feng X-S, Zhang R-J, Zhang L, Mu Y-D, Hao J-C, Qian D-J, Lou Y-F, 2004. Mineralization mechanism of calcium phosphates under three kinds of Langmuir monolayers. Langmuir20, 2243–9. [PubMed: 15835677]

Zhang L, Balcerzak M, Radisson J, Thouverey C, Pikula S, Azzar G, Buchet R, 2005. Phosphodiesterase Activity of Alkaline Phosphatase in ATP-initiated Ca 2+ and Phosphate Deposition in Isolated Chicken Matrix Vesicles. J. Biol. Chem280, 37289–37296. 10.1074/jbc.M504260200 [PubMed: 16147995]

Zhao W, Wang Z, Xu Z, Sahai N, 2018. Osteocalcin facilitates calcium phosphate ion complex growth as revealed by free energy calculation. Phys. Chem. Chem. Phys20, 13047–13056. 10.1039/c8cp01105b [PubMed: 29713719]

Zou Z, Tang T, Macías-Sánchez E, Sviben S, Landis WJ, Bertinetti L, Fratzl P, 2020. Three-dimensional structural interrelations between cells, extracellular matrix, and mineral in normally mineralizing avian leg tendon. Proc. Natl. Acad. Sci201917932. 10.1073/pnas.1917932117

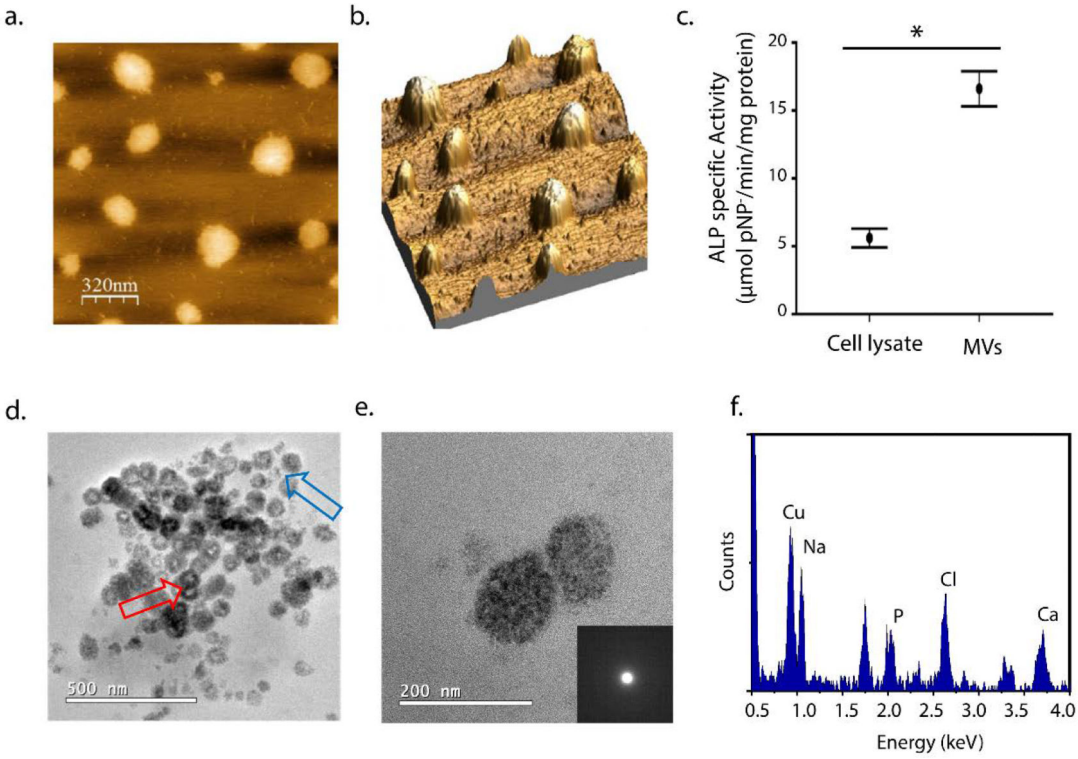

Figure 1.

Characterization of MVs extracted from chicken embryo femurs: (a) AFM images by height distribution and (b) 3D projection of the isolated MVs on mica. (c) ALP specific activity for cell lysate and MVs fractions (µmol pNP^{-}/min/mg protein). Values are presented as mean ± standard error and statistical significance was assessed with t-tests (*$p < 0.05$). (d) TEM images of the MVs after 24 h of mineralization in SCL (2 mM $CaCl_2$ and 3.42 mM NaH_2PO_4) at 37°C. (e) Enlarged TEM image of a pair of mineralized-vesicles and their respective amorphous-like SAED and (f) the respective EDS spectrum indicating the presence of Ca and P. The presence of Na and Cl is also observed due to the large amount of NaCl in the SCL and Cu is from de TEM grid.

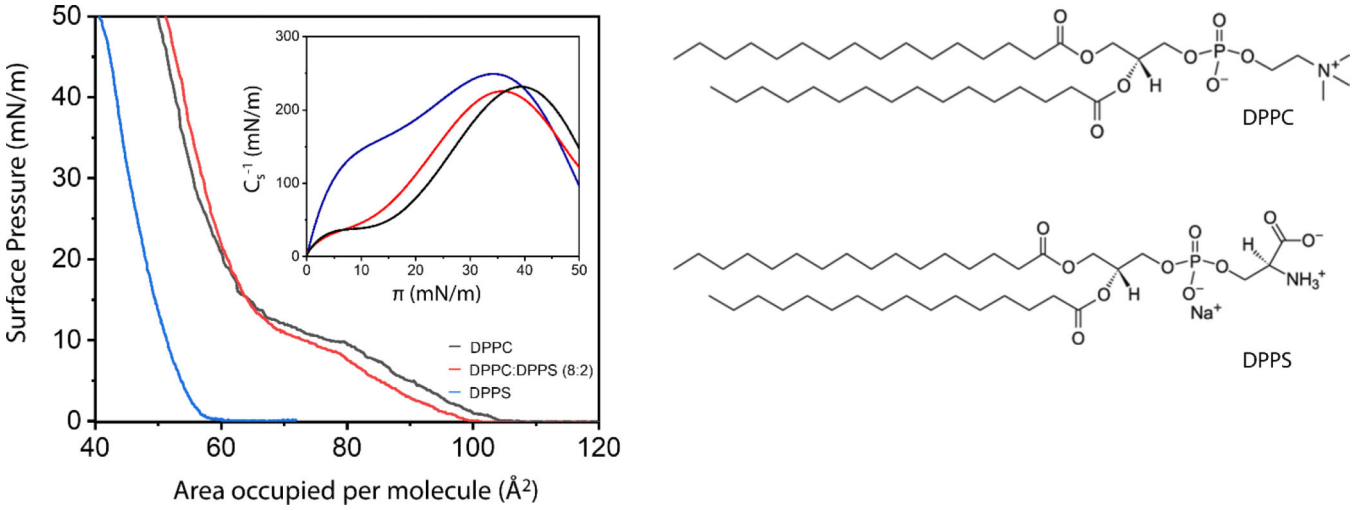

Figure 2.

π -A isotherms of DPPC (black line), DPPC:DPPS (8:2, molar ratio) (red line) and DPPS (blue line) monolayers in subphase containing m-SCL solution, at 25°C. Inset depicts the C_s^{-1} *vs* π curves for the monolayers. Right panel: chemical structures of DPPC and DPPS lipids.

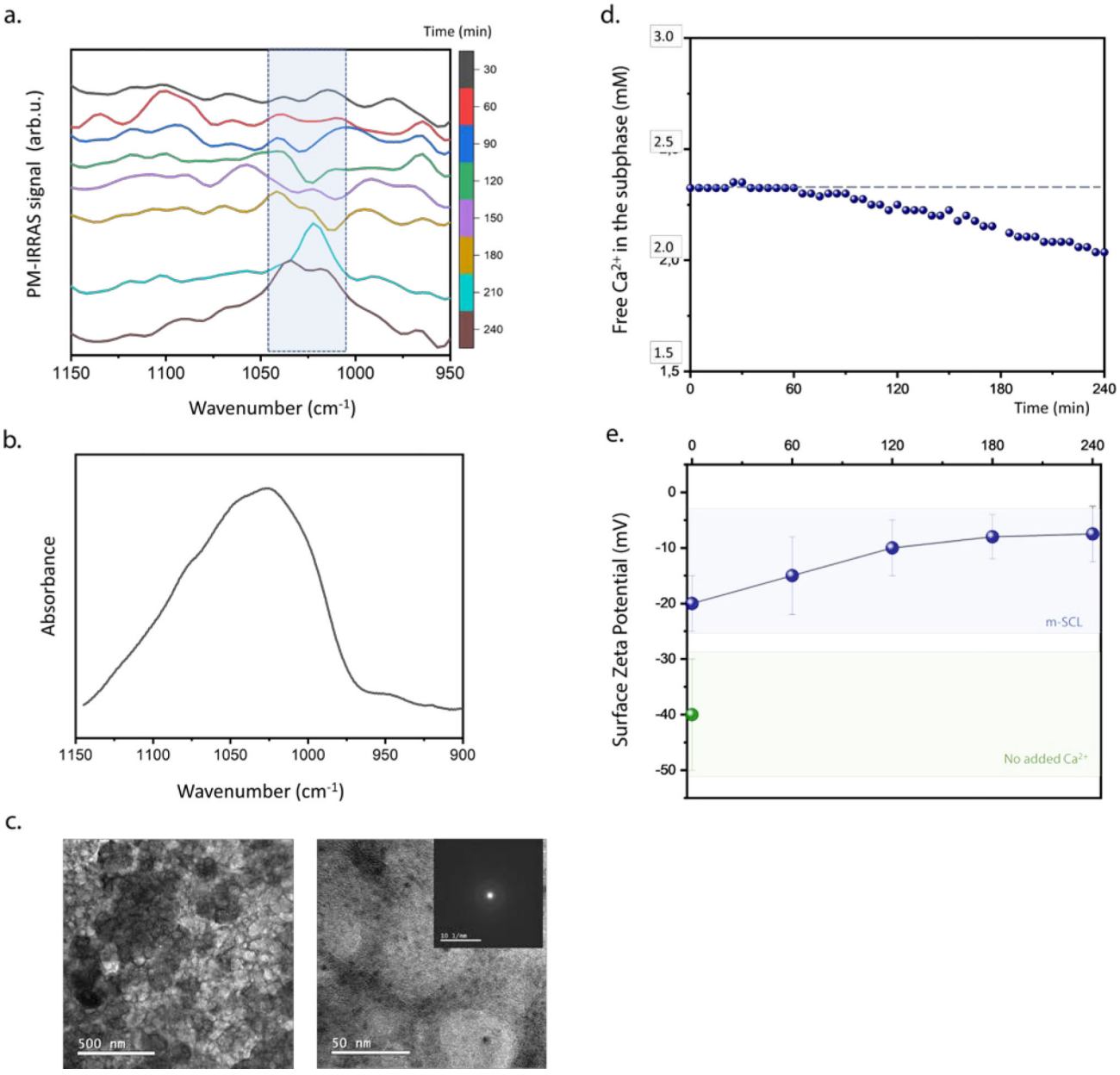

Figure. 3.

DPPS monolayers control calcium phosphate nucleation at the air-liquid interface. (a) PM-IRRAS spectra in the 1150–950 cm^{-1} range for the DPPS monolayer in subphase composed of the m-SCL mineralizing buffer (pH 7.4), at 25°C and π = 30 mN/m. Spectra were obtained at different time intervals for a period of 240 min. Blue box in the spectra highlighted the region between 1045–1010 cm^{-1} assigned to the absorption bands of evolving inorganic phosphate group. (b) FTIR spectrum in the region of ν_3 PO_4^{3-} absorption obtained for the material collected from the monolayer of DPPS after 240 min of mineralization. (c) TEM images and SAED (inset) of DPPS monolayers transferred to Cu-grids after 240 min. (d) Potentiometric measurement of $[Ca^{2+}]_{free}$ in the subphase below

the DPPS monolayer. (c) *Ex-situ* analysis of surface ζ-potential of DPPS monolayers in absence of Ca^{2+} ions and after different mineralization time points (blue dots).

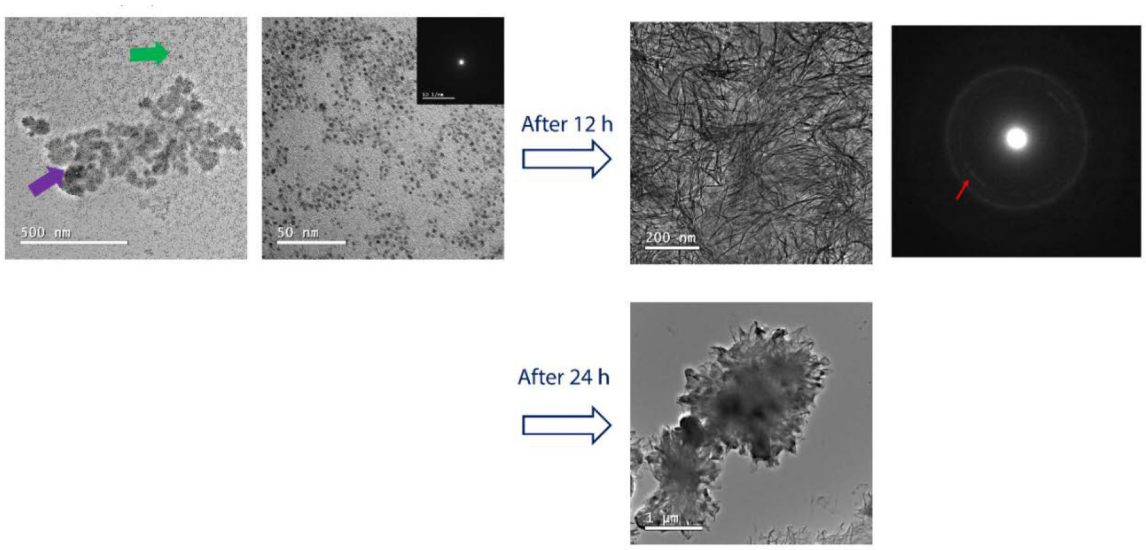

Figure 4.

Morphology of DPPS-enriched monolayers after mineralization. TEM images and their respective SAED electron diffraction patterns for the monolayers of DPPC:DPPS (8:2) molar ratio, transferred after 240 min of mineralization at 25°C. For the mixed DPPC:DPPS monolayer, the presence of nanometric complexes (~ 5 nm) indicated by the green arrow aggregates into larger structures (purple arrow). It is observed that these initially amorphous complexes crystallize after 12 h (red arrow in the SAED pattern). The formation of micrometric aggregates and a complete rupture of the transferred monolayer is observed after 24 h.

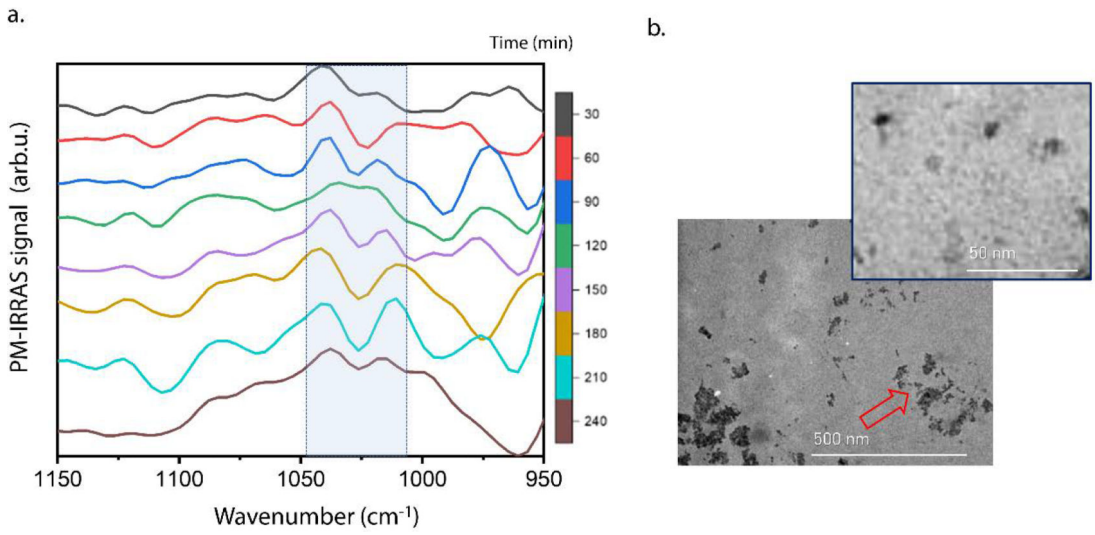

Figure 5.

Mineralization mediated by Langmuir monolayers composed of lipids extracted from MVs. (a) PM-IRRAS spectra in the region between 1150–950 cm^{-1} for the monolayer formed by the lipid extract of MVs, in subphase composed of the m-SCL mineralizing buffer (pH 7.4), at 25°C and π = 30 mN/m. Spectra were obtained at different time intervals for a period of 240 min. Blue boxes in the spectra highlight the region between 1045–1010 cm^{-1} assigned to the absorption bands of evolving inorganic phosphate group. (b) TEM images for the monolayer formed by the lipid extract of MVs transferred after 4 hours of mineralization at 25°C.

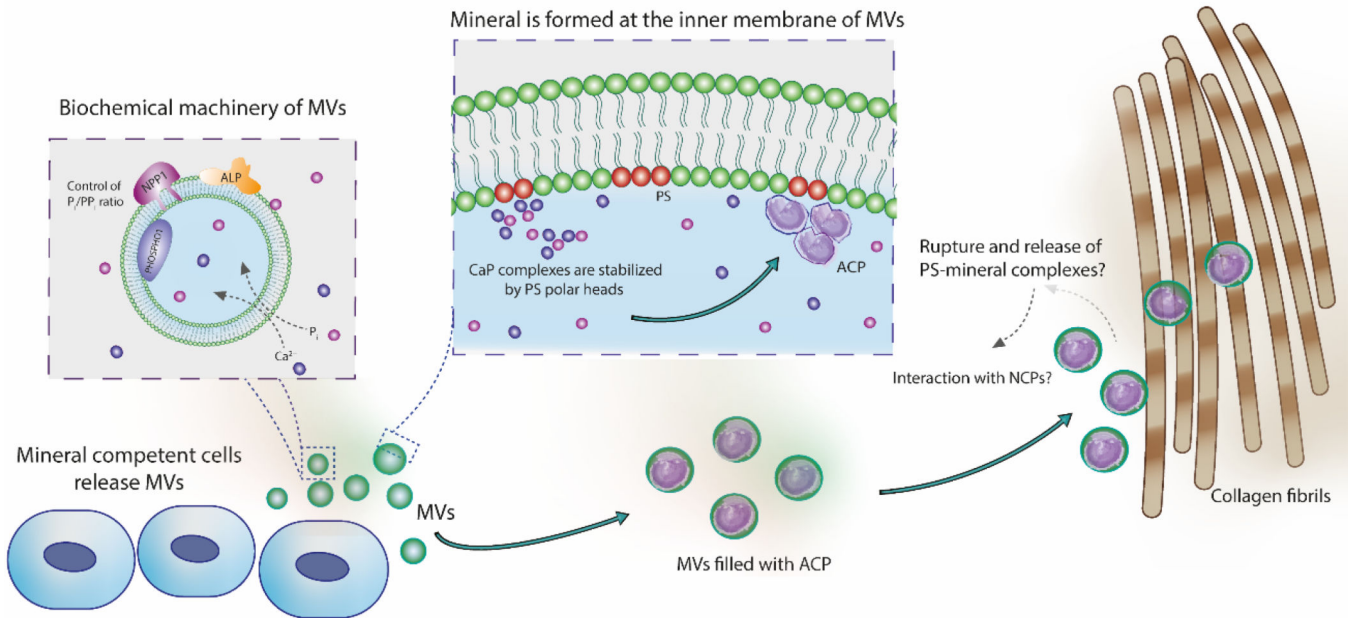

Figure 6.

Role of MVs in the nucleation of calcium phosphates and in the mineralization of collagen fibrils. Mineral-competent cells release MVs harboring an enzymatic machinery capable of controlling the phosphate/pyrophosphate ratio required to trigger mineralization. These vesicles are rich on phosphatidylserine (PS) in their lumen, creating a highly negatively charged interface for nucleation and stabilization of calcium phosphate complexes. These complexes evolve to the formation of ACP, the very first mineral phase in the MVs. Vesicles filled with ACP could directly infiltrate within the collagen fibrils scaffold and then transform to platelet-like crystals. This direct amorphous-apatite transformation has been proposed *in vitro* using confined polymer domains (Lotsari et al., 2018) and similar structures (i.e. mineralized globules) has been observed in the collagen scaffold of zebra fish fin tails (Mahamid et al., 2010) and avian leg tendon (Zou et al., 2020). Then, MVs could breakdown and release their components to the mineralizing front, either by mechanical stress or actions of phospholipases (Wu et al., 2002). Phospholipases are highly active enzymes in the growth plate (Mebarek et al., 2013). This process could release phospholipid-mineral complexes (associated or not with proteins) to direct the infiltration of biomineral precursor phase in the *gap* region of collagen through a mechanism similar to the proposed for non-collagenous proteins (Nudelman et al., 2010). Alternatively, these phospholipid-mineral complexes could interact with non-collagenous proteins and then be directed to the collagen matrix for mineralization.